PCCP

Multiscale Solvation Effect on Reactivity of β-O-4 of Lignin Dimers in Deep Eutectic Solvents

Journal:	*Physical Chemistry Chemical Physics*
Manuscript ID	CP-ART-09-2021-004342.R1
Article Type:	Paper
Date Submitted by the Author:	25-Oct-2021
Complete List of Authors:	Qiao, Qi; University of Kentucky, Chemical and Materials Engineering Shi, Jian; University of Kentucky, Biosystems and Agricultural Engineering Shao, Qing; University of Kentucky, Chemical and Materials Engineering

ARTICLE

Multiscale Solvation Effect on Reactivity of β-O-4 of Lignin Dimers in Deep Eutectic Solvents

Received 00th January 20xx,
Accepted 00th January 20xx

DOI: 10.1039/x0xx00000x

Qi Qiao,[a] Jian Shi [b] and Qing Shao *[a]

Deep eutectic solvents (DESs) emerge as a medium to enhance the depolymerization of lignin. One critical question is how the solvation of lignin in DES may affect the reactivity of lignin. To shed light on this question, we investigate the solvation of four lignin dimers in three DES solutions using molecular dynamics simulations and quantum mechanical calculations. The four lignin dimers are composed of guaiacyl and syringyl units and used as the model for lignin. The three DES solutions are composed of choline, Cl^- and three acids: lactic acid, levulinic acid and oxalic acid. We investigate the preferential accumulation of individual DES components in the solvation shells and the exporsure area and electrostatic potential of β-O-4 linkage of four lignin dimers in the three DESs. The results show that DES could influence the affinity and nucleophilicity of β-O-4 linkage through three effects: (1) forming a charged solvation shell, (2) varying exposure of β-O-4 linkage and (3) adjusting the electrostatic potential of β-O-4 linkage. Our simulations indicate a comprehensive and multiscale effect of DESs on lignin decomposition.

1. Introduction

Coproducing chemicals from lignin and biofuels from cellulose and hemicellulose can greatly improve the technoeconomic feasibility of a biorefinery technology that contributes to the sustainability of the society.[1-8] One challenge is to design a solvent that can facilitate the decomposition of lignin in a mild condition.[9-11] Deep eutectic solvents (DESs) emerge as a promising candidate for this purpose. DESs are composed of organic hydrogen bond donors (HBDs) and hydrogen bond acceptors (HBAs).[12-19]

However, it remains unclear how the solvation effect affects the decomposition of lignin in DES through the breakdown of the major interunit linkages such as β-O-4, β-β, and β-5, etc. We could design suitable candidates from the vast chemical space of DESs if we better understood the solvation feature of lignin in DESs and how these features may affect the reactivity of lignin.[20-22]

One question is about the distribution of DES components and ions within the solvation shell of lignin. A DES is essentially a multi-component mixture. Some solvent molecules and ions may prefer to accumulate around lignin. The uneven accumulation of DES compounds and ions may form a charged solvation shell around the lignin dimer. This charged solvation shell then could create a thermodynamic barrier for lignin-catalyst binding.

The second question is about the exposure level of the β-O-4 linkage of lignin. The β-O-4 linkage is a crucial point to break lignin. The nearby molecules and ions in the solvation shell may adjust the exposure area of β-O-4 linkages and allow the catalysts to approach them.

The third question is about the effect of the charged solvation shell on the electrostatic potential of β-O-4 linkage. The electrostatic potential of β-O-4 linkage reflects the potential of β-O-4 linkage to be decomposed by certain catalysts. The solvation of DESs may adjust the electrostatic potential of a β-O-4 linkage and its potential to be decomposed.

Quite a few studies have indicated the promising role of DESs in assisting the dissolution and decomposition of lignin and other biomass components.[23-32] Muley et al.[33] investigated the biomass and lignin depolymerization using choline chloride (ChCl)-based DESs with oxalic acid, lactic acid and formic acid. They found that oxalic acid and formic acid show the highest lignin yield at specific conditions. Additional microwave heating promotes selective bond cleavage such as β-O-4 linkage. Malaeke et al.[27] reported that lignin shows high solubility in ChCl-based DESs using ultrasound irradiation. Tan et al.[28] found that ChCl: lactic acid (1:15) and ChCl: formic acid (1:2) could extract more than 60 wt% of lignin and exhibited comparable reactivity of the lignin. Di Marino et al.[29] investigated the depolymerization of lignin in ChCl: urea (1:2) combined with electrochemical oxidative depolymerisation. Their method could produce low molecular weight products and could be further extracted using liquid-liquid extraction. Sosa et al.[34] reported that the solubility of kraft lignin increases most in ChCl-based DES with 1,6-hexanediol and maleic acid. They also found that carboxylic acid-based DES could cleave β-O-4, α-O-4 and α-O-α bonds, whereas alcohol-based DES helps maintain the lignin structure.

This work presents our effort of investigating the solvation effect on decomposition potential of lignin in DESs using

[a] Department of Chemical and Materials Engineering, University of Kentucky, Lexington, Kentucky 40506, United States. E-mail: qshao@uky.edu
[b] Department of Biosystems and Agricultural Engineering, University of Kentucky, Lexington, Kentucky 40506, United States.

quantum mechanical (QM) calculation and molecular dynamics (MD) simulations. We focus on the reactivity of β-O-4 because it is considered as the dominant and the most liable interunit linkage in native lignin in common biomass feedstocks.[2, 8, 35] Based on the three questions above, we plan to investigate the solvation effect on the decomposition potential of lignin from three aspects: (a) the chemicophysical features of molecules in the solvation shell, (b) the exposure of β-O-4, and (c) the electrostatic potential surface around β-O-4.

We select four lignin dimers and three DESs as the model system. The four lignin dimers are composed of guaiacyl (G) and syringyl (S) units and these units combine with each other by β-O-4 linkage (G-G, G-S, S-G, S-S).[36-38] The three choline based DESs are: (a) ChCl: Lactic acid (1:2) (Lac12), (b) ChCl: Levulinic acid (1:2) (Lev12), and (c) ChCl: Oxalic acid (1:1) (Oxa11). The rest of the paper will be organized as follows: section 2 will present the detail of the model and simulation, section 3 will present the result and discussion and section 4 will present a conclusion.

2. Molecular model and simulation detail

2.1 Molecular dynamics simulations

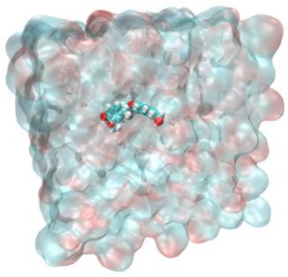

Figure 1. Snapshot of the initial configuration for G-G-Lac12 containing 200 choline, 200 Cl^-, and 400 lactic acid molecules. The G-G lignin dimer is shown in the VDW model and other molecules and ions are shown in QuickSurf model (C: cyan: O: red, N: blue, H: white, and Cl^-: brown)

The simulation systems were created by placing a lignin dimer in the center of a cubic box and filling the box with specific numbers of solvent molecules and ions (choline, lactic acid, levulinic acid, oxalic acid and Cl^-). All-atom models are used to describe the lignin dimer, choline and acid molecules. Figure 1 shows a snapshot of a G-G lignin dimer in a box of ChCl: lactic acid (1:2) solution (G-G-Lac12). Table 1 lists the numbers of solution molecules and the simulation box sizes in the twelve simulation boxes. Figure S1 shows the detailed configurations and chemical sketches of the four lignin dimers. Figure S2 shows the detailed configurations and chemical sketches of the DES components.

A three-step simulation process is carried out for each system: (1) an energy minimization to remove any too-close contact between atoms, (2) a 700-ns isobaric-isothermal (NPT, P=1 atm, T=373K) ensemble molecular dynamics (MD) simulation to help the system reach thermodynamic equilibrium, (3) a 500-ns NPT (P=1 atm, T=373 K) ensemble MD simulation for data collection with a frequency of 50-ps. An integral step of 2 fs is employed in Steps (2) and (3). The Berendsen method[1] is used to control the system pressure, and the velocity rescaling method[2] is used to control the system temperature. All simulations utilize the periodic boundary conditions.

Table 1. Detail of the solvent molecules in the twelve simulation systems.

System	# of Choline	# of Cl^-	# of Acid	Box size (nm^3)
G-G-Lac12	200	200	400	$4.6 \times 4.6 \times 4.6$
G-G-Lev12	200	200	400	$4.9 \times 4.9 \times 4.9$
G-G-Oxa11	200	200	200	$4.0 \times 4.0 \times 4.0$
G-S-Lac12	200	200	400	$4.6 \times 4.6 \times 4.6$
G-S-Lev12	200	200	400	$4.9 \times 4.9 \times 4.9$
G-S-Oxa11	200	200	200	$4.0 \times 4.0 \times 4.0$
S-G-Lac12	200	200	400	$4.6 \times 4.6 \times 4.6$
S-G-Lev12	200	200	400	$4.9 \times 4.9 \times 4.9$
S-G-Oxa11	200	200	200	$4.0 \times 4.0 \times 4.0$
S-S-Lac12	200	200	400	$4.6 \times 4.6 \times 4.6$
S-S-Lev12	200	200	400	$4.9 \times 4.9 \times 4.9$
S-S-Oxa11	200	200	200	$4.0 \times 4.0 \times 4.0$

The nonbonded and bonded interactions in the system were described using the OPLSAA/M force field[3]. The force field parameters were assigned using the LigParGen web server[4-6]. The short- and long-range nonbonded interactions used in the OPLS-AA/M force field are calculated using the Lennard-Jones 12-6 and Coulomb potential, respectively (equation 1).

$$E = \sum_i \sum_{j<i} \left\{ \frac{1}{4\pi\varepsilon_0} \frac{q_i q_j e^2}{r_{ij}} + 4\varepsilon_{ij} \left[\left(\frac{\sigma_{ij}}{r_{ij}} \right)^{12} - \left(\frac{\sigma_{ij}}{r_{ij}} \right)^{6} \right] \right\} \qquad (1)$$

where r_{ij} is the distance between atom *i* and *j*, q_i *and* q_j are the partial charges of atom *i* and *j*, ε_0 is the free space permittivity, ε_{ij} and σ_{ij} are energetic and geometric parameters. The particle mesh Ewald[7] (PME) sum is used to calculate long-range potentials, and the LINCS algorithm[8] is used to constrain bonds involving hydrogen atoms. The energy minimization and MD simulations were conducted using GROMACS 2020.4[9] for all twelve systems.

2.2 Quantum mechanical calculation:

The configurations in which the β-O-4 present the largest SASA from MD step (3) are used to generate the initial configurations for the quantum mechanical calculations. The initial configuration includes the lignin dimer and any solvent molecules within 0.5 nm from the oxygen atoms of the β-O_4 of the lignin dimer. Figure S3 shows the configurations used in this work. The single-point calculation is carried out at the B3LYP/6-311+G** level of theory using Gaussian 16 Rev. A.03 package[10] with SCF convergence and ultrafine integration grids. The population analysis method of Hirshfeld[11] is used to calculate the atomic charges of the oxygen atom of the β-O_4. The D3 version of Grimme's dispersion with Becke-Johnson damping[12] (GD3BJ) is used to improve the accuracy of the results by accounting for long-range van der Waals interactions.

3. Results and discussion

3.1 Solvation shell of lignin dimer

The net charge of the solvation shell is overwhelmingly positive for the four lignin dimers in the three DESs (Figure 2). The net charge distributions are calculated based on the configurations of 10000 frames. The net charge is the sum of the partial charges of the ions and molecules that have a heavy atom within a distance of 0.5 nm from the heavy atom on the lignin dimer. The heavy atom is defined as any carbon, oxygen, nitrogen atom or Cl^- ions of lignin dimers and DES components. The cutoff of 0.5 nm is defined by oxygen-oxygen radial distribution function (RDF) of lignin dimer and DES components. Figure S4 shows an example of O-O RDF of G-G-Lac12 system. Figure S5-S8 shows the distribution of net charge, solvent molecules and ions of the solvation shell around the β-O-4 linkage of lignin dimers in three DESs. As shown in Figure 2, the majority of the curves are positive. These distributions indicate that the lignin dimers are surrounded by a cationic shell in most scenarios in the three DESs.

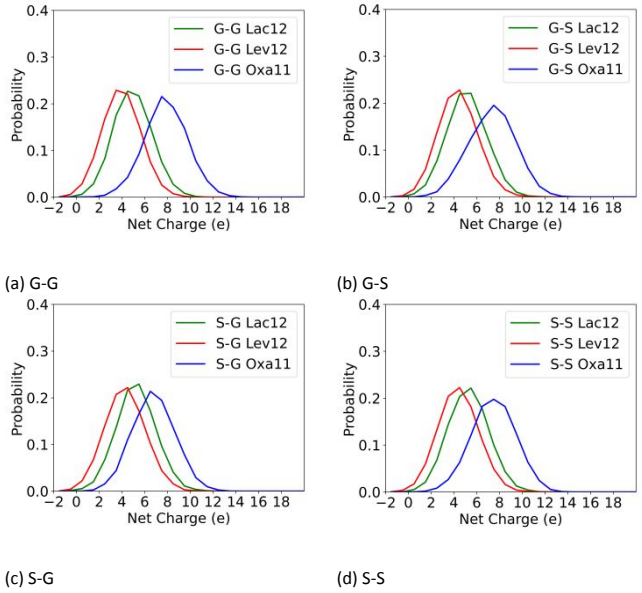

Figure 2. The distribution of net charge of the solvation shell around (a) G-G, (b) G-S, (c) S-G and (d) S-S lignin dimers in three DESs.

The scale of the solvation shell net charge relies more on the type of DES than the type of the lignin dimer. As shown in Figure 2a, the scale of solvation shell net charge for G-G shifts from [-2, 10] to [2, 14] as the DES changes from Lev12 to Oxa11. The other three lignin dimers present a similar trend with the variation of DES, as shown in Figure 2b-d. The variation of lignin types does not present a similar trend. As shown in Figure 2a-d, the solvation shell net charge scale remains around [-2, 10] for the four lignin dimers in Lac12. Similar phenomena could be found for the four lignin dimers in the other two DESs.

It is worth notifying that the lignin dimers present a very small chance to possess a negatively charged solvation shell in the Lac12 and Lev12. As shown in Figure 2, the lignin dimers have around 0.28%-0.63% chance to possess a negatively charged solvation shell. The percentages drop to 0.02%-0.14% in Lac12 while almost zero in Oxa11. Table S1 lists the chance of a negatively charged solvation shell for the twelve systems. Figure S9-S12 shows the solvation shell net charge as a function of time.

The charged solvation shell could be due to the preferential accumulation of charged DES compounds around the lignin dimers. Figure 3 shows the average numbers of molecules and ions within the solvation shell of the lignin dimers in the three DESs. The number of choline (7-16) is larger than the Cl^- (3-8). The preferential accumulation is recognized as a major factor that makes the non-bulk feature for solutions.[39-45] Here, the preferential accumulation makes a charged solvation shell for lignin dimers in a charge-neutral solution. The difference in the net charge scales indicates that preferential accumulation depends more on the DES than the lignin dimer. The wide range of the net charge scale indicates the dynamics of the solvation shell.

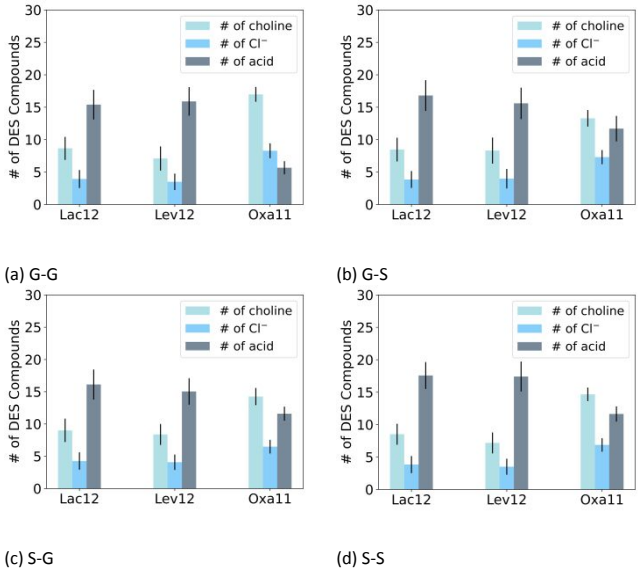

Figure 3. The number of the solvent molecules and ions of the solvation shell around (a) G-G, (b) G-S, (c) S-G and (d) S-S lignin dimers in three DESs.

The lignin dimers could associate with DES molecules within the solvation shell by hydrogen bonds (HBs). Here we only consider the HBs between lignin dimer and organic DES components: HBs of lignin-acid and lignin-choline. Table 2 lists the average number of total lignin-DES hydrogen bonds (lignin-acid + lignin-choline) per lignin dimer. Figure 4 shows the distribution of number of HBs for both lignin-acid and lignin-choline of G-G in three DESs. The HBs distribution of the other three lignin dimers are shown in Figure S13-S15.

Table 2. The average number of total lignin-DES hydrogen bonds (lignin-acid + lignin-choline) per lignin dimer for the lignin dimer in the three DESs.

	Lac12	Lev12	Oxa11
G-G	1.45±1.15	1.45±1.15	0.91±0.86
G-S	1.47±1.15	1.47±1.15	1.15±0.99
S-G	1.56±1.20	1.56±1.20	1.42±1.02
S-S	1.59±1.20	1.59±1.20	1.26±1.06

The average number of total lignin-dimer HBs is only around one per lignin dimer during the 500-ns simulation (Table 2). Figure 4 shows that the number of HBs of lignin-acid (blue) and

lignin-choline (red) varies from 0 to 1 mostly for G-G in the three DESs. The lignin dimer prefers to form HBs with acid rather than choline molecules (Figure 4). Figure 4c shows that the number of HBs of lignin-acid is slightly larger than the lignin-choline even the number of choline molecules is about twice of the acid molecules for Oxa11. Similar phenomena could be observed for all the other lignin dimers in three DESs (Figure S13-S15).

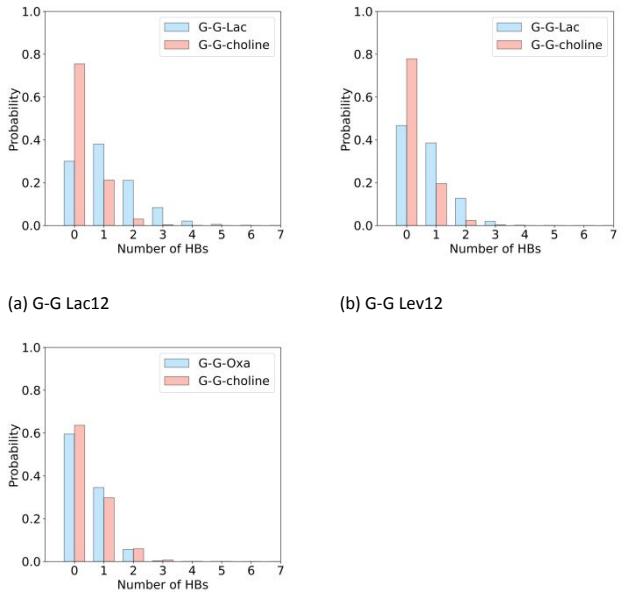

(a) G-G Lac12 (b) G-G Lev12

(c) G-G Oxa11

Figure 4. The distribution of HBs of lignin-acid and lignin-choline of (a) G-G Lac12, (b) G-G Lev12 and (c) G-G Oxa11. The HBs distribution of the other lignin dimers are shown in Figure S13-S15.

The preferential accumulation of the charged solvation shell may be due to the hydrophobic association instead of hydrogen bonds. The lignin dimers could associate with DES molecules by two non-bond interactions: hydrogen bonds and hydrophobic associations. The analysis reveals that the total average number of lignin-DES HBs is only around one per lignin dimer (Table 2). This value scale is much lower than the number of molecules (26-31) near the lignin dimers (Figure 3). Thus, the hydrogen bonds are less likely to determine the preferential accumulation. Alternatively, hydrophobic associations may play an essential role in the preferential accumulations. Two groups, Youngs et al.[31] and D'Agostino et al.[32], have reported that the solvation of glucose in the ionic liquid of 1-ethyl-3-methylimidazolium acetate is mainly affected by the hydrogen bonding and anion ($[OAc]^-$) instead of cations. Such a difference between the solvation of glucose and lignin dimer indicates that we should consider different solvation effects when designing DES for biomass decomposition processes.

The important role of the hydrophobic association in preferential accumulations is also supported by that the lignin dimers prefer hydrophobic molecules rather than hydrophilic ones. Both the lactic acid and levulinic acid have hydrophobic parts such as $-CH_2-CH_2-$ or $-CH_3$, whereas oxalic acid only has hydrophilic groups of -COOH. Therefore, the lactic acid and levulinic acid molecules prefer to stay in the solvation shell more than the oxalic acid molecules. More choline and Cl^- molecules are preferred in the solvation shell of lignin dimer in Oxa11 (Figure 3).

The charged solvation shell will create a thermodynamic barrier for lignin-catalyst binding affinity. The solvation shell has been recognized as a determining thermodynamic barrier for substrate-substrate affinity in solvent.[46, 47] The charged solvation shell may influence the lignin-catalyst affinity from two aspects. First, the charged solvation shell may create a local electric field that attracts or repulses the catalyst. Second, the catalyst may need to compensate a thermodynamic penalty for repealing the DES molecules in the charged solvation shell so that it can get access to the lignin. The variation of the net charge distribution in Figure 2 implies that the thermodynamic barrier should present a dynamic fluctuation in the system, and we could tune this thermodynamic barrier by adjusting the DES formula.

3.2 Exposure area of β-O-4 linkage

We then investigate the exposure area of β-O-4 of lignin dimer using solvent accessible surface areas (SASA). The SASA is calculate by tracing the center of a probe sphere (radius = 0.14 nm) rolling over the oxygen atom of β-O-4. As discussed above, the catalysts or the reactants should get access to β-O-4 to break the linkage. A larger SASA value indicates more exposure area of β-O-4 and a higher chance for the catalysts to get access to the linkage. Figure 5 shows the distributions of SASA of β-O-4 for the four lignin dimers in the three DESs with an r=0.14 nm probe. The SASA of β-O-4 for the four lignin dimers ranges from 0 to 0.167 nm^2. We used the same procedure to calculate the SASA of oxygen on the backbone of a short peptide EAKA. The SASA of oxygen ranges from 0.034 to 0.817 nm^2. Figure S17-S20 shows the SASA of the β-O-4 linkage as a function of time.

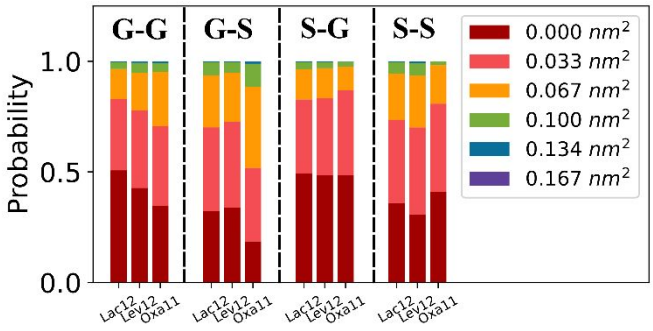

Figure 5. The distribution of SASA of β-O4 for the four lignin dimers in the three DESs. The probe radius r=0.14 nm. Figure S16 shows the distribution of SASA with a probe radius r=0.10 nm.

The SASA distribution depends on both lignin dimer and DES. As shown in Figure 5, G-S dimer has the highest probability of exposure area ≥ 0.100 nm^2 (0.06), whereas S-G shows the lowest probability (0.04) in Lac12 systems. The S-S dimer shows the highest probability of exposure area ≥ 0.100 nm^2 (0.07) and the S-G dimer shows the lowest probability of 0.03 in Lev12. The highest probability of the β-O-4 linkage with SASA ≥ 0.100 nm^2 is G-S lignin dimer in Oxa11 (0.12), while the lowest probability is S-S lignin dimer in Oxa11 (0.02). Such a change of SASA

indicates that we could design DES to control the exposure of β-O-4 between specific types of monomers.

The analysis of SASA reveals that maximizing the exposure of β-O-4 may be one of the remaining challenges in lignin depolymerization in DESs. As shown in Figure 5, the probability for β-O-4 SASA ≥ 0.10 nm^2 is only about 0.02 to 0.12 for all the four types of lignin dimer in three DESs. If we consider 0.1 nm^2 as the threshold, this low value for probability indicates that the other parts of the lignin cover the β-O-4 linkage most of the time. However, it also suggests the possibility of designing suitable DESs to control the exposure of β-O-4. This exposure should relate to the conformation-free energy landscape of lignin dimer. The DES molecules and their preferential accumulation should influence this conformation-free energy landscape. Thus, we could design DESs to improve the exposure of β-O-4 and enhance its possibility to be decomposed. In addition, the analysis of SASA shows that the β-O-4 between different monomers present different exposure tendencies in the three DESs. We could select the type of β-O-4 to break by changing the DES.

3.3 Electrostatic potential of β-O-4 linkage

At last, we investigate the solvation effect on the electrostatic potential of β-O-4 using QM calculations.[48] For all 12 cases, we select the configuration in which the β-O-4 present the largest SASA. This selection is determined based on the hypothesis that a larger SASA may indicate a higher chance for the β-O-4 to be accessed. Each configuration includes the whole lignin dimer and any ions and molecules within 0.5 nm of β-O-4. We take this compromise because the configuration with the whole solvation shell is beyond our current computational capacity. Figure S3 shows the snapshots of the 12 cases. We calculate the atomic partial charge of the 12 configurations using Hirshfeld because this method can well characterize the nucleophilicity of β-O-4 linkage.[49] Table 3 shows the atomic partial charge of the oxygen of β-O-4 for four lignin dimers in three DESs. It has been reported that the cleavage of β-O-4 linkage should relate to its electrostatic potential.[2, 50, 51] A more negative value indicates easier to cleave the β-O-4 linkage of the lignin dimer, and a higher chance for lignin to be decomposed.

Table 3. The atomic partial charge of β-O-4 for the four lignin dimers in the three DESs.

	Lac12	Lev12	Oxa11
G-G	-0.125	-0.116	-0.152
G-S	-0.132	-0.141	-0.134
S-G	-0.124	-0.133	-0.144
S-S	-0.141	-0.140	-0.122

The atomic partial charges of β-O-4 relates to both DESs and lignin dimer types. As listed in Table 3, the partial charge of G-G dimer shifts from -0.125 to -0.152, decreased by around 20% when the DES changes from Lac12 to Oxa11. The partial charges of the other three dimers also vary when changing DESs. The four lignin dimers present different partial charges in the same DESs. Taking Lac12 for example, the value of S-S dimers is 12% lower than that of G-G dimer.

The variation of atomic partial charges indicates the possibility of developing DESs to selectively break specific β-O-4 linkage. As shown in Table 3, no single DES presents the lowest partial charges for all four lignin dimers and no single lignin dimer presents the lowest atomic partial charges in all three DESs. Therefore, the most breakable β-O-4 linkage should vary in the three DESs. In addition, the order of atomic partial charges also varies in the three DESs. The order is S-S < G-S < G-G < S-G in Lac 12, while the order is G-G < S-G < G-S < S-S in Oxa11. If the lower partial charge implies a β-O-4 linkage easier to break, among the four dimers, the S-S is the easiest to break and the S-G is the most stable in Lac12, while the S-S turns out to be the most stable and G-G is the easiest to break in Oxa11.

4. Conclusion

In summary, this work reveals three solvation effects of DES molecules on decomposition potential of lignin. The first two are at the molecular level. The DES molecules compose a positively charged solvation shell around the lignin. This solvation shell could make a thermodynamic barrier for lignin-catalyst binding. The solvation could affect the exposure level of β-O-4 and further influence the potential of catalysts to get access to the desired site. The third is the quantum effect of the solvation. The solvation changes the electrostatic potential of β-O-4. Such a change in electrostatic potential would affect the potential of the chemical bond to be broken. The three effects consist of a comprehensive relationship between the DES composition and its ability to enhance the decomposition of lignin. This comprehensive relationship would explain the various experimental observations of lignin pretreatment and decomposition in DES. Such a comprehensive and multiscale relationship would challenge the design of a suitable DES because the design must balance all the three effects. However, this relationship also provides the opportunity to design DES to decompose lignin on specific chemical bonds. Such selective decomposition could increase the yield of desired products.

Conflicts of interest

There are no conflicts to declare.

Acknowledgements

Qi Qiao and Qing Shao acknowledge the support from the Startup Funds of the University of Kentucky. Jian Shi acknowledges the support from the National Science Foundation under Cooperative Agreement No. 1632854 and the National Institute of Food and Agriculture, U.S. Department of Agriculture, Sustainability Challenge Area grant under accession number 1015068. We would like to thank the University of Kentucky Center for Computational Sciences and Information Technology Services Research Computing for their support and use of the Lipscomb Compute Cluster and associated research computing resources.

Notes and references

1. J. Zakzeski, P. C. Bruijnincx, A. L. Jongerius and B. M. Weckhuysen, *Chemical reviews*, 2010, **110**, 3552-3599.
2. Z. Sun, B. Fridrich, A. de Santi, S. Elangovan and K. Barta, *Chemical reviews*, 2018, **118**, 614-678.
3. C. O. Tuck, E. Pérez, I. T. Horváth, R. A. Sheldon and M. Poliakoff, *Science*, 2012, **337**, 695.
4. M. V. Galkin and J. S. M. Samec, *ChemSusChem*, 2016, **9**, 1544-1558.
5. H. Long, X. Li, H. Wang and J. Jia, *Renewable and Sustainable Energy Reviews*, 2013, **26**, 344-352.
6. S. Behera, R. Arora, N. Nandhagopal and S. Kumar, *Renewable and sustainable energy reviews*, 2014, **36**, 91-106.
7. M. Rastogi and S. Shrivastava, *Renewable and Sustainable Energy Reviews*, 2017, **80**, 330-340.
8. M. P. Pandey and C. S. Kim, *Chemical Engineering & Technology*, 2011, **34**, 29-41.
9. G. T. Beckham, C. W. Johnson, E. M. Karp, D. Salvachúa and D. R. Vardon, *Current opinion in biotechnology*, 2016, **42**, 40-53.
10. R. Singh, A. Shukla, S. Tiwari and M. Srivastava, *Renewable and Sustainable Energy Reviews*, 2014, **32**, 713-728.
11. C. Chio, M. Sain and W. Qin, *Renewable and Sustainable Energy Reviews*, 2019, **107**, 232-249.
12. B. B. Hansen, S. Spittle, B. Chen, D. Poe, Y. Zhang, J. M. Klein, A. Horton, L. Adhikari, T. Zelovich and B. W. Doherty, *Chemical reviews*, 2020, **121**, 1232-1285.
13. P. Xu, G.-W. Zheng, M.-H. Zong, N. Li and W.-Y. Lou, *Bioresources and bioprocessing*, 2017, **4**, 1-18.
14. A. E. Ünlü, A. Arıkaya and S. Takaç, *Green Processing and Synthesis*, 2019, **8**, 355-372.
15. A. Shishov, A. Bulatov, M. Locatelli, S. Carradori and V. Andruch, *Microchemical Journal*, 2017, **135**, 33-38.
16. M. Zdanowicz, K. Wilpiszewska and T. Spychaj, *Carbohydrate polymers*, 2018, **200**, 361-380.
17. A. P. Abbott, D. Boothby, G. Capper, D. L. Davies and R. K. Rasheed, *Journal of the American Chemical Society*, 2004, **126**, 9142-9147.
18. G. Di Carmine, A. P. Abbott and C. D'agostino, *Reaction Chemistry & Engineering*, 2021, **6**, 582-598.
19. A. P. Abbott, G. Capper, D. L. Davies, R. K. Rasheed and V. Tambyrajah, *Chemical communications*, 2003, 70-71.
20. L. Shuai and J. Luterbacher, *ChemSusChem*, 2016, **9**, 133-155.
21. M. A. Mellmer, C. Sener, J. M. R. Gallo, J. S. Luterbacher, D. M. Alonso and J. A. Dumesic, *Angewandte chemie international edition*, 2014, **53**, 11872-11875.
22. M. A. Mellmer, C. Sanpitakseree, B. Demir, P. Bai, K. Ma, M. Neurock and J. A. Dumesic, *Nature Catalysis*, 2018, **1**, 199-207.
23. W. Wang and D.-J. Lee, *Bioresource Technology*, 2021, **339**, 125587.
24. B. Ai, W. Li, J. Woomer, M. Li, Y. Pu, Z. Sheng, L. Zheng, A. Adedeji, A. J. Ragauskas and J. Shi, *Green Chemistry*, 2020, **22**, 6372-6383.
25. H. Ji and P. Lv, *Green chemistry*, 2020, **22**, 1378-1387.
26. S. Wang, H. Li, L.-P. Xiao and G. Song, *Frontiers in Energy Research*, 2020, **8**, 48.
27. H. Malaeke, M. R. Housaindokht, H. Monhemi and M. Izadyar, *Journal of molecular liquids*, 2018, **263**, 193-199.
28. Y. T. Tan, G. C. Ngoh and A. S. M. Chua, *Bioresource technology*, 2019, **281**, 359-366.
29. D. Di Marino, D. Stöckmann, S. Kriescher, S. Stiefel and M. Wessling, *Green Chemistry*, 2016, **18**, 6021-6028.
30. Z. Chen, X. Bai and C. Wan, *ACS Sustainable Chemistry & Engineering*, 2018, **6**, 12205-12216.
31. T. G. Youngs, J. D. Holbrey, C. L. Mullan, S. E. Norman, M. C. Lagunas, C. D'Agostino, M. D. Mantle, L. F. Gladden, D. T. Bowron and C. Hardacre, *Chemical Science*, 2011, **2**, 1594-1605.
32. C. D'Agostino, M. D. Mantle, C. L. Mullan, C. Hardacre and L. F. Gladden, *ChemPhysChem*, 2018, **19**, 1081-1088.
33. P. D. Muley, J. K. Mobley, X. Tong, B. Novak, J. Stevens, D. Moldovan, J. Shi and D. Boldor, *Energy Conversion and Management*, 2019, **196**, 1080-1088.
34. F. H. Sosa, D. O. Abranches, A. M. da Costa Lopes, J. A. Coutinho and M. C. da Costa, *ACS Sustainable Chemistry & Engineering*, 2020, **8**, 18577-18589.
35. H. Wang, M. Tucker and Y. Ji, *J. Appl. Chem*, 2013, **2013**.
36. J. Ralph, *Phytochemistry Reviews*, 2010, **9**, 65-83.
37. J. Ralph, K. Lundquist, G. Brunow, F. Lu, H. Kim, P. F. Schatz, J. M. Marita, R. D. Hatfield, S. A. Ralph and J. H. Christensen, *Phytochemistry reviews*, 2004, **3**, 29-60.
38. J. Ralph, M. Bunzel, J. M. Marita, R. D. Hatfield, F. Lu, H. Kim, P. F. Schatz, J. H. Grabber and H. Steinhart, *Phytochemistry Reviews*, 2004, **3**, 79-96.
39. S. Rozas, M. Atilhan and S. Aparicio, *The Journal of Physical Chemistry B*, 2020, **124**, 1197-1206.
40. N. Zec, G. Mangiapia, M. L. Zheludkevich, S. Busch and J.-F. Moulin, *Physical Chemistry Chemical Physics*, 2020, **22**, 12104-12112.
41. M. Atilhan and S. Aparicio, *Journal of Molecular Liquids*, 2019, **283**, 147-154.
42. Q. Gao, N. Wu, Y. Qin, A. Laaksonen, Y. Zhu, X. Ji and X. Lu, *Journal of Molecular Liquids*, 2020, **319**, 114298.
43. M. Shakourian-Fard, S. M. Taimoory, H. R. Ghenaatian, G. Kamath and J. F. Trant, *Journal of Molecular Liquids*, 2021, **327**, 114850.
44. Z. Tan, Y. Peng, J. Liu, Y. Yang, Z. Zhang, Z. Chen, B. Mao and J. Yan, *ChemElectroChem*, 2020, **7**, 4601-4605.
45. A. Elbourne, N. Meftahi, T. L. Greaves, C. F. McConville, G. Bryant, S. J. Bryant and A. J. Christofferson, *Journal of Colloid and Interface Science*, 2021, **591**, 38-51.
46. D. Chandler, *Nature*, 2005, **437**, 640-647.
47. J. He, H. Zhang, T. Yue, W. Sun, Y. Hu and C. Zhang, *Langmuir*, 2021, **37**, 2205-2212.
48. B. Wang, C. Rong, P. K. Chattaraj and S. Liu, *Theoretical Chemistry Accounts*, 2019, **138**, 1-9.
49. F. L. Hirshfeld, *Theoretica chimica acta*, 1977, **44**, 129-138.
50. G. E. Klinger, Y. Zhou, J. A. Foote, A. M. Wester, Y. Cui, M. Alherech, S. S. Stahl, J. E. Jackson and E. L. Hegg, *ChemSusChem*, 2020, **13**, 4394.
51. C. Xu, R. A. D. Arancon, J. Labidi and R. Luque, *Chemical Society Reviews*, 2014, **43**, 7485-7500.